

# Embedding initial data for black hole collisions

by

Joseph D. Romano and Richard H. Price  
Department of Physics  
University of Utah  
Salt Lake City UT 84112

## Abstract

The visualization of curved sections of spacetime can be of considerable conceptual value. We discuss here the visualization of initial data for the problem of the head-on collision of two black holes. The problem of constructing the embedding diagram is explicitly presented for the best studied initial data, the Misner geometry. We present a partial solution of the embedding diagrams and discuss issues related to completing the solution.

PACS number(s): 0420, 0240, 0270, 9760L

## 1. Introduction

A benchmark for numerical relativity has been the computation of the gravitational radiation waveforms generated by the collision of two Schwarzschild throats starting from rest[1]. This description of the starting configuration is not complete. One can choose initial data in many ways to fit this verbal description. What remains to be specified can be said to correspond to the initial mutual distortion of the holes or the long-wavelength radiation present on the initial hypersurface. (Initial short wavelength radiation would presumably be “obvious.”) When the initial separation of the throats is sufficiently small, a single nearly-spherical horizon surrounds both throats, and the exterior geometry can be thought of as a perturbation of a single Schwarzschild throat. Recent studies[2] show that this viewpoint is reasonably successful even when the horizon is highly distorted or is even split into two disjoint horizons. The extent to which the initial geometry mixes its “two throat” and “one throat” nature is the key to understanding this

perturbation approach which promises to be important in the future. One would like to get a feeling for how this changes with changing separation of the throats, with different choices of initial data for a given separation, etc. For these, and many other reasons, it would be very useful to have a direct way of visualizing initial data. Indeed, computer visualization would seem most appropriate for data that has been the starting point for so much intensive numerical computation.

This would certainly seem possible in principle. The initial data under discussion are all momentarily stationary, so—in appropriate 4-dimensional coordinates—the initial time rate of change of the metric is zero; the initial data then consists only of the initial 3-geometry. Since that geometry is rotationally symmetric about the symmetry axis along which the holes will move, we can take a slice through that axis. The initial data is then fully specified by the spatial 2-geometry on that slice. A curved 2-geometry can, at least locally, be represented isometrically by a curved surface in flat Euclidean 3-space. Due to the nature of the black hole initial data one supposes such a surface to have the general shape of a pair of trousers. Such pictures in fact are commonly drawn, but the actual surface, to our knowledge, has never been computed.

In the present paper we discuss the generation of an embedding diagram for the most commonly used black hole initial data, the “Misner data” [3]. On rather general grounds we show that the generation of the embedding cannot proceed smoothly. We show explicitly that for the Misner geometry the breakdown takes the form of the mathematical equivalent of shock waves in the embedding surface. This breakdown occurs, however, only quite near the crotch of the trousers and does not stop us from computing most of the embedding surface. This “partial” embedding is sufficient for most aspects of visualization of the initial data. In a subsequent paper we will report on the extent to which it is possible to overcome the obstacles to a global embedding.

The remainder of the paper is organized as follows: Section 2 introduces the mathematical preliminaries for the general problem of embedding a curved 2-dimensional geometry in Euclidean 3-space. Special emphasis is given to the case where the equations are everywhere hyperbolic since that turns out to be the case for the Misner geometry, which is described in Sec. 3. Numerical results are given in Sec. 4 along with a description of how the solution of the embedding breaks down at the formation of a “shock.” In Sec. 5

we discuss whether these shocks are inevitable and, if they are, how the incomplete embedding diagrams can be of use. As a specific example, we show how they aid in the understanding of the range of validity of perturbation theory.

## 2. The mathematics of embedding: The Darboux equation

Consider a positive-definite, 2-dimensional geometry described in terms of local coordinates  $(x, y)$  and line element

$$ds^2 = E dx^2 + 2F dx dy + G dy^2. \quad (1)$$

We would like to realize this abstract 2-geometry as a curved surface in flat Euclidean 3-space, subject to the condition that the line element induced on the surface by the flat Euclidean geometry agrees with that of (1). We want, in other words, to find three functions  $(U, V, W)$  such that

$$du^2 + dv^2 + dw^2 = E dx^2 + 2F dx dy + G dy^2 \quad (2)$$

when  $u = U(x, y)$ ,  $v = V(x, y)$ ,  $w = W(x, y)$  are substituted into the left hand side of the above equation. This requirement leads to three conditions

$$E = U_{,x}^2 + V_{,x}^2 + W_{,x}^2 \quad (3)$$

$$F = U_{,x}U_{,y} + V_{,x}V_{,y} + W_{,x}W_{,y} \quad (4)$$

$$G = U_{,y}^2 + V_{,y}^2 + W_{,y}^2 \quad (5)$$

where  $U_{,x}$  means partial derivative of  $U$  with respect to  $x$ , etc. The functions  $(U, V, W)$  are called embedding functions, and the mapping  $(x, y) \rightarrow (U, V, W)$  defines a 2-dimensional surface in the  $(u, v, w)$  Euclidean 3-space. A set of functions  $(U, V, W)$  satisfying (3)-(5) is referred to in the mathematical literature as a locally isometric embedding. Our goal is to find such an embedding for the 2-geometry corresponding to the Misner initial data.

Rather than try to solve the above system of nonlinear, first-order partial differential equations (PDEs) for the unknowns  $(U, V, W)$ , we will take a different approach originally due to Darboux. (See, for example, [4].) This will lead to a single, nonlinear, second-order PDE for the embedding function  $W(x, y)$ . Although the resulting equation is nonlinear in the second partial

derivatives of  $W$ , it is of a special type and can be reduced to a characteristic system of five quasilinear, first-order PDEs. It is this system of equations which we then try to solve numerically. Once we find  $W$ , the other embedding functions  $U$  and  $V$  are determined, in terms of  $W$ , by means of quadratures. The purpose of the remainder of this section (and the appendix at the end of the paper) is to make these statements more precise.

Consider, instead of (1), the 2-dimensional line element

$$du^2 + dv^2 = (E dx^2 + 2F dx dy + G dy^2) - dw^2. \quad (6)$$

Substituting  $w = W(x, y)$  into the right hand side of the above equation, we find

$$du^2 + dv^2 = (E - W_{,x}^2) dx^2 + 2(F - W_{,x}W_{,y}) dx dy + (G - W_{,y}^2) dy^2. \quad (7)$$

Without loss of generality, we can assume that  $W_{,x}$  and  $W_{,y}$  vanish at the point about which we are trying to find the locally isometric embedding. (We can always perform a Euclidean transformation—i.e., a translation and rigid rotation—to guarantee that this is actually the case.) Since  $du^2 + dv^2$  is positive-definite, and hence nondegenerate, in a neighborhood of that point, it follows that (1) must be nondegenerate for it to be locally embeddable. The left hand side of (7) is also flat, and hence has vanishing Gaussian curvature. (There are no additional geometric constraints. In two dimensions, the Riemann curvature tensor is determined completely by the scalar curvature, and the Gaussian curvature equals one-half the scalar curvature.) If we express the Gaussian curvature of (7) in terms of the appropriate first and second partial derivatives of the components

$$(E - W_{,x}^2), \quad (F - W_{,x}W_{,y}), \quad (G - W_{,y}^2) \quad (8)$$

we find

$$\mathcal{A}(rt - s^2) + \mathcal{B}r + \mathcal{C}s + \mathcal{D}t + \mathcal{E} = 0 \quad (9)$$

where  $\mathcal{A}, \mathcal{B}, \mathcal{C}, \mathcal{D}, \mathcal{E}$  are complicated functions of  $E, F, G$  and their first and second partial derivatives, and of the first partial derivatives  $p := W_{,x}$  and  $q := W_{,y}$  of  $W$ . (See the appendix for explicit expressions for  $\mathcal{A}, \mathcal{B}, \dots, \mathcal{E}$ .) Here  $r, s, t$  are shorthand notations for the second partial derivatives  $W_{,xx}, W_{,xy}, W_{,yy}$ . All third derivatives of  $W$  cancel when calculating the Gaussian curvature of (7). A second-order PDE of the general form (9), with  $\mathcal{A}, \mathcal{B}, \dots, \mathcal{E}$  independent of  $r, s, t$ , is said to be of the Monge-Ampère type.

It differs from the general, second-order PDE in that the only nonlinearity in  $r, s, t$  occurs in the combination  $(rt - s^2)$ . This special feature results in a number of important simplifications below. In the context of the embedding problem—with  $\mathcal{A}, \mathcal{B}, \dots, \mathcal{E}$  depending on  $E, F, G$  as in the appendix—equation (9) is called the Darboux equation.

If we write the general, nonlinear, second-order PDE for the unknown  $W(x, y)$  as

$$Q(x, y, W, p, q, r, s, t) = 0 \quad (10)$$

then the characteristic curves  $(x(\lambda), y(\lambda))$  are those for which

$$Q_{,r} \left( \frac{dy}{d\lambda} \right)^2 - Q_{,s} \left( \frac{dx}{d\lambda} \right) \left( \frac{dy}{d\lambda} \right) + Q_{,t} \left( \frac{dx}{d\lambda} \right)^2 = 0. \quad (11)$$

The discriminant

$$\Delta := Q_{,s}^2 - 4Q_{,r}Q_{,t} \quad (12)$$

determines whether real solutions exist for  $(x(\lambda), y(\lambda))$ . An equation is said to be hyperbolic for regions in which  $\Delta > 0$ , so that two directions exist for characteristics at each point in the region. The equation is said to be elliptic for  $\Delta < 0$ , and parabolic for  $\Delta = 0$ .

In the case of the Monge-Ampère equation

$$Q_{,t} = \mathcal{D} + \mathcal{A}r \quad (13)$$

$$Q_{,s} = \mathcal{C} - 2\mathcal{A}s \quad (14)$$

$$Q_{,r} = \mathcal{B} + \mathcal{A}t \quad (15)$$

yielding

$$\Delta = \mathcal{C}^2 - 4\mathcal{B}\mathcal{D} + 4\mathcal{A}\mathcal{E}. \quad (16)$$

The above expression for  $\Delta$  does not contain  $r, s$ , or  $t$ .

In the case of the Darboux equation,  $\Delta$  has a remarkable geometric property: It can be written in terms of the Gaussian curvature  $K$  of the original line element in (1):

$$\Delta = -16 K (EG - F^2)^3 (n^3)^2. \quad (17)$$

(Here  $n^3$  is the  $w$ -component of the unit normal to the embedded surface. See the appendix for details.) For a positive-definite 2-geometry,  $EG - F^2 > 0$  and the sign of  $\Delta$  is determined by the Gaussian curvature  $K$ . For  $K > 0$  the

Darboux equation is elliptic, so there are no characteristic curves. This means that features on one part of the embedding surface influence all other parts of the embedding. As we will show in the next section and in the appendix, the 2-geometry for the Misner initial data has everywhere-negative Gaussian curvature. In this case, the Darboux equation is hyperbolic, and features, such as the choice of boundary conditions for the embedding, propagate along characteristics and remain fairly localized.

A geometric meaning for the characteristics of the Darboux equation emerges if we use (13)-(15) and the expressions for  $\mathcal{A}, \mathcal{B}, \dots, \mathcal{E}$  given in the appendix to rewrite (11) as

$$\begin{aligned} & Q_{,r} \left( \frac{dy}{d\lambda} \right)^2 - Q_{,s} \left( \frac{dx}{d\lambda} \right) \left( \frac{dy}{d\lambda} \right) + Q_{,t} \left( \frac{dx}{d\lambda} \right)^2 \\ &= -4n^3(EG - F^2) \left[ K_{11} \left( \frac{dx}{d\lambda} \right)^2 + 2K_{12} \left( \frac{dx}{d\lambda} \right) \left( \frac{dy}{d\lambda} \right) + K_{22} \left( \frac{dy}{d\lambda} \right)^2 \right]. \end{aligned}$$

Here  $K_{11}, K_{12}, K_{22}$  are the  $(x, y)$ -components of the extrinsic curvature tensor  $\mathbf{K}$  for the embedding (see the appendix). The characteristic directions for the 2-geometry of (1) are thus seen to be the zero vectors (i.e., asymptotic directions) of  $\mathbf{K}$ ; they are the vectors  $\vec{v}$  for which  $\vec{v} \cdot \mathbf{K} \cdot \vec{v} = 0$ . Clearly, for  $K < 0$  there are two principal curvatures of opposite sign. The principal directions are orthogonal in the geometry of (1) and it is easy to see that the characteristic directions must be symmetrically arranged with respect to the principal directions. That is, a principal direction must bisect the angle between a pair of characteristics.

Since we are guaranteed that there exist two characteristics through any point, we can use the characteristics themselves as coordinates. We label one family of characteristics (i.e., one family of solutions of (11)) with  $\alpha$  and the other family with  $\beta$ . The Darboux equation can then be reformulated in terms of five unknown functions  $(x, y, W, p, q)$  of the variables  $(\alpha, \beta)$ . It is shown in the appendix that these are determined by the five quasilinear, first-order PDEs

$$\frac{1}{2}(\mathcal{C} - \delta) x_{,\alpha} - \mathcal{B} y_{,\alpha} - \mathcal{A} q_{,\alpha} = 0 \quad (18)$$

$$\frac{1}{2}(\mathcal{C} + \delta) x_{,\beta} - \mathcal{B} y_{,\beta} - \mathcal{A} q_{,\beta} = 0 \quad (19)$$

$$\frac{1}{2}(\mathcal{C} + \delta) y_{,\alpha} - \mathcal{D} x_{,\alpha} - \mathcal{A} p_{,\alpha} = 0 \quad (20)$$

$$\frac{1}{2}(\mathcal{C} - \delta) y_{,\beta} - \mathcal{D} x_{,\beta} - \mathcal{A} p_{,\beta} = 0 \quad (21)$$

$$W_{,\alpha} - p x_{,\alpha} - q y_{,\alpha} = 0 \quad (22)$$

where  $\delta := \sqrt{\Delta}$ . (It should be noted that the general, nonlinear, second-order hyperbolic PDE, in characteristic form, requires eight equations for the eight unknowns  $(x, y, W, p, q, r, s, t)$ . It is the special nature of the Monge-Ampère equation that results in a system of only five equations[5].)

Of the three embedding functions  $(U, V, W)$ , the Darboux approach singles out one,  $W$ . It turns out, as shown in the appendix, that the remaining steps to complete the embedding are fairly straightforward. Once the solutions to (18)-(22) are found, the remaining embedding functions  $U, V$  are determined in terms of  $W$  by means of quadratures[6].

To close this section, we point out that the method of Darboux described above is only one of many approaches to solving the embedding problem. There is an extensive Russian mathematical literature on locally isometric embeddings for negative Gaussian curvature 2-geometries which describes the method of Riemann invariants. Interested readers should see the review article by Poznyak and Shikin[7] for more information. Also, a paper by Bernstein[8] describes an iterative numerical scheme for computing isometric embeddings.

### 3. The Misner geometry

The black hole initial data used for numerical relativity studies[1] is the Misner 3-geometry[3] given by

$$ds_{\text{Misner}}^2 = a^2 \varphi_{\text{Misner}}^4 \left[ d\mu^2 + d\eta^2 + \sin^2 \eta d\phi^2 \right] \quad (23)$$

where

$$\varphi_{\text{Misner}} = \sum_{n=-\infty}^{\infty} \frac{1}{\sqrt{\cosh(\mu + 2n\mu_0) - \cos \eta}}. \quad (24)$$

The geometry has a total ADM mass

$$M_{\text{tot}} = 4a \sum_{n=1}^{\infty} \frac{1}{\sinh(n\mu_0)} \quad (25)$$

and describes two throats located near  $\mu = \pm\mu_0$ . A measure of the separation of the throats is  $L$ , the proper distance from  $\mu = -\mu_0$  to  $\mu = +\mu_0$ , which can be shown to be

$$L = 2a \left( 1 + 2\mu_0 \sum_{n=1}^{\infty} \frac{n}{\sinh(n\mu_0)} \right). \quad (26)$$

The constant  $a$  is a scaling factor that sets the size of both  $M_{\text{tot}}$  and  $L$ , but not the ratio  $L/M_{\text{tot}}$ , and does not affect the “shape” of the geometry. The only parameter affecting the shape is  $\mu_0$ , which is an increasing function of  $L/M_{\text{tot}}$ . For  $\mu_0 \ll 1$  there is a single, nearly spherical, initial horizon; for  $\mu_0 \gg 1$  the geometry represents two widely separated throats, each with an initial horizon. The transition from a single horizon to a split horizon with two disjoint segments occurs at  $\mu_0 \approx 1.8$ .

The Misner 3-geometry is rotationally symmetric—i.e., it is independent of the azimuthal angle  $\phi$ . We therefore lose no geometric information by taking a  $\phi = \text{const}$  slice of (23), thereby arriving at a 2-geometry

$$ds^2 = a^2 \varphi_{\text{Misner}}^4 \left[ d\mu^2 + d\eta^2 \right] \quad (27)$$

and the possibility of an embedding in Euclidean 3-space.

A numerical study of the Gaussian curvature  $K$  of this 2-geometry (27) shows that the Gaussian curvature is everywhere-negative. We have also been able to write the Gaussian curvature in a form in which it is manifest that it is everywhere-negative:

$$K = -\frac{1}{2} a^{-2} \varphi_{\text{Misner}}^{-6} \sum_{m=-\infty}^{\infty} \sum_{n=-\infty}^{\infty} \frac{\cosh(2\mu_0(m-n)) - 1}{[\cosh(\mu + 2m\mu_0) - \cos \eta]^{3/2} [\cosh(\mu + 2n\mu_0) - \cos \eta]^{3/2}}.$$

(See the appendix for details.)

For our analysis, it is convenient to transform from the  $(\mu, \eta)$  coordinates to coordinates better suited to the description of the geometry at large distances from the holes. To do this we transform from  $(\mu, \eta)$  to  $(\theta, R)$ , as if from bispherical to polar coordinates, according to

$$\theta = \arctan \left( \frac{\sin \eta}{\sinh \mu} \right) \quad (28)$$

$$R = \frac{a}{\cosh \mu - \cos \eta} \sqrt{\sinh^2 \mu + \sin^2 \eta}. \quad (29)$$



The inverse transformation formulae are

$$\mu = \pm \operatorname{arccosh} \left( \frac{R^2 + a^2}{\sqrt{(R^2 + a^2)^2 - (2aR \cos \theta)^2}} \right) \quad (30)$$

$$\eta = \pm \operatorname{arccos} \left( \frac{R^2 - a^2}{\sqrt{(R^2 - a^2)^2 + (2aR \sin \theta)^2}} \right). \quad (31)$$

The signs are determined by requiring that  $\mu > 0$  for  $-\pi/2 < \theta < +\pi/2$  and  $\eta > 0$  for  $0 < \theta < \pi$ . In terms of the  $(\theta, R)$  coordinates, the 2-geometry (27) takes the form

$$ds^2 = \Phi^4(\theta, R) (R^2 d\theta^2 + dR^2) \quad (32)$$

with

$$\Phi = 1 + \frac{a}{R} \sum_{n \neq 0} \frac{1}{|\sinh(n\mu_0)| \sqrt{1 + (2a/R) \coth(n\mu_0) \cos \theta + (a^2/R^2) \coth^2(n\mu_0)}}. \quad (33)$$

If we identify  $(\theta, R)$  with  $(x, y)$ , then the coefficients  $E, F, G$  of the line element (1), which we take as the starting point for the embedding problem, are given by

$$E = R^2 \Phi^4(\theta, R) \quad (34)$$

$$F = 0 \quad (35)$$

$$G = \Phi^4(\theta, R). \quad (36)$$

Since  $K < 0$  for the Misner 2-geometry, the corresponding Darboux equation is hyperbolic and appropriate Cauchy data must be specified. We choose to specify “initial” data at large constant  $R$ . Here the 2-geometry (32) is approximately that of a single, central Schwarzschild throat, and  $R$  plays the role of the Schwarzschild isotropic radius.  $R$  is related to the Schwarzschild curvature radius  $r_{\text{curv}}$  via

$$R = \frac{1}{2} r_{\text{curv}} \left( 1 - M_{\text{tot}}/r_{\text{curv}} + \sqrt{1 - 2M_{\text{tot}}/r_{\text{curv}}} \right) \quad (37)$$

where  $M_{\text{tot}}$  is the total ADM mass (25) of the single, central Schwarzschild throat. Equivalently,

$$r_{\text{curv}} = R (1 + M_{\text{tot}}/2R)^2. \quad (38)$$

For a single Schwarzschild throat of mass  $M_{\text{tot}}$ , the embedding is given by

$$W = 2M_{\text{tot}} \left( \sqrt{2R/M_{\text{tot}}} - \sqrt{M_{\text{tot}}/2R} \right). \quad (39)$$

The initial values of  $W, p, q, r, s, t$  on the  $R = \text{const}$  surface are found from (39) and its derivatives with respect to  $\theta$  and  $R$ .

Our numerical approach is a finite-difference solution to the characteristic equations in (18)-(22). On the  $R = \text{const}$  initial value surface, grid points are chosen to be equally spaced in  $\theta$ . A pair of  $(\alpha, \beta)$  characteristics is then started from each initial grid point. Equations (18)-(22) are used to propagate  $(x, y, W, p, q)$  forward along the characteristics. The two axes of bilateral symmetry of the Misner geometry are used to reduce the size of the numerical grid by a factor of four. The infinite sums were approximated by finite sums from  $-N_{\text{sum}}$  to  $N_{\text{sum}}$ , with  $N_{\text{sum}}$  large enough so that the omitted terms were negligible.

## 4. Results: Characteristics and partial embeddings for the Misner geometry

Equations (18)-(22) were solved numerically, and from the results, solutions were constructed for  $U(\alpha, \beta), V(\alpha, \beta)$ . With these solutions and the solution for  $W(\alpha, \beta)$ , the two families of characteristics in the  $(u, v, w)$  space are known. The results are shown in Fig. 1 in the three cases  $\mu_0 = 1, 2, 3$  which correspond to  $L/M_{\text{tot}} = 1.92, 3.88, 7.92$ . In these figures and in all those below, the value of the scaling constant  $a$  was chosen, for each value of  $\mu_0$ , so that  $M_{\text{tot}} = 1$ . The  $(u, v)$  coordinates therefore measure distances in units of  $M_{\text{tot}}$ , so that in the figures we are always visually comparing spacetimes with the same total mass, but with throats at different separation.

An immediately apparent, and crucial, feature of the figures is that the characteristic net does not cover the complete  $(u, v)$  interior to the  $R = \text{const}$  initial value surface. The numerical solution inevitably breaks down at the boundary of an oval region that includes the throats. This is not a numerical artifact; extensive numerical testing confirmed that the location of the breakdown was reasonably independent of numerical step size.

A breakdown is, in fact, mathematically inevitable. This can most easily be seen by imagining the characteristics at the midpoint of the  $(u, v)$  plot. Since the underlying 2-geometry is symmetric about the rotation axis, the

embedding diagram must be reflection symmetric about the horizontal line through the midpoint. The symmetry axis, then, must be a principal direction of the extrinsic curvature. The zero directions of  $\mathbf{K}$ , and hence the directions of the characteristics, must be symmetrically arranged about the principal direction. The nature of the characteristics must therefore be that shown in Fig. 2. But what direction along these characteristics is the “forward” direction of propagation of information from the boundary? A choice of direction along these characteristic segments violates the symmetry of the boundary. The direction of forward propagation must be ill-defined at the midpoint. An extension of this argument shows that this must be a problem not only at the midpoint but also, at least, on the symmetry axis joining the throats. The inescapable conclusion is that the characteristic net emanating from the  $R = \text{const}$  boundary cannot smoothly and continuously cover the entire region inside the boundary and outside the throats.

This conclusion, in fact, does not depend on the symmetry of the Misner geometry, but only on its general topological character. We can shrink the  $R = \text{const}$  boundary, and the throats, so that the embedding region becomes a 2-sphere with three singular points, representing the boundary and each of the throats. Let us suppose that we can put a single family of characteristics on this 2-sphere, starting from the boundary and ending only at the throats. The tangent vectors to the characteristics (pointing in the direction of propagation of the solution) constitute a vector field having no singularities or zeroes except at the boundary and at the throats. At the boundary, the tangent vectors all point outward, while at the throats, they all point inward (if the specification of additional boundary conditions is to be avoided). The index of the vector field[9] would then be +1 at each of these points, and the total index of the vector field would equal 3. But the Poincaré index theorem[9] requires that the index of a vector field on a manifold equal the Euler characteristic  $\chi$  of the manifold. For a 2-sphere, the Euler characteristic  $\chi = 2$ , so the tangent field to the family of characteristics is impossible. A simple generalization of this argument shows that problems must develop in the embedding of negative Gaussian curvature initial data for any number of holes other than unity.

It remains to determine the precise nature of the inescapable breakdown in the propagation of the characteristics. It cannot be due to a geometric singularity. The *intrinsic* geometry of the embedded surface is fixed, of course, by the requirement that it be isometric to the nonsingular Misner 2-

geometry. We are carefully studying the *extrinsic* geometry of the embedded surface that we generate numerically, and we have found no evidence, so far, that any singularity is developing as the characteristics approach the point of breakdown.

The actual nature of the breakdown is suggested by our argument above about the incompatible directions of characteristics. The breakdown occurs when characteristics of the same family cross each other, as in the classic example of shocks in gas flow. At such crossings there are three characteristic directions (two from the crossed characteristics, and one from the characteristic of the other family) and the propagation of the solution cannot proceed. Figure 3 shows a detail of the numerical results for the propagation of characteristics in the extreme case  $\mu_0 = 6$ . To the left of the crossing at  $u \approx 6.6, v \approx 8.2$  the results are valid; to the right, the results are meaningless.

Although the development of these “embedding shocks” (i.e., characteristic crossings) block the computation of the embedding in an inner region of the geometry, we can still compute the outer region and obtain most of the visually useful information. Figure 4 shows the outline of the embedded surface (a view along the  $v$  axis) for the cases  $\mu_0 = 1$  and  $\mu_0 = 3$ . A clear geometric distinction is apparent. For the  $\mu_0 = 3$  case, the structure close in (in the region  $-5 < u < 5$ ) is that of two throats. On a larger scale the geometry takes on the character of a single Schwarzschild throat. The shape of the  $\mu_0 = 1$  case is quite different. Though it has the same “trousers” topology as that of  $\mu_0 = 3$ , the steep sides of the embedding near  $u = \pm 2$  mean that there is no region in which the individual throats look like more-or-less isolated holes. A 3-dimensional plot of the  $\mu_0 = 3$  geometry is presented in Fig. 5.

## 5. Discussion

The development of “embedding shocks” is the most interesting feature of the problem of embedding the everywhere-negative Gaussian curvature Misner 2-geometry. The primary question to be asked about them is whether it is inevitable that a “forbidden region” develop towards the crotch of the embedding, cut off from the outer region by the embedding shock. The topological arguments of the previous section clearly establish that *something* must go wrong with the characteristics, but the failure could be confined to the symmetry axis joining the throats, at which the characteristics meet with

incompatible directions of forward propagation. In effect, the “forbidden region” could be degenerate, with zero area. This is not, of course, what our numerical results show, but the location of the embedding shock depends on the initial data. A correct small change in the initial data might shift the location of the embedding shock inward, reducing the area of the forbidden region; the precisely correct initial data might even reduce the forbidden region to a line. We have numerically studied the effect on the shock location of the precise form of the initial data. The results strongly suggest that no improvement of the Cauchy data can significantly reduce the size of the forbidden region. [There is an additional point that must be added in connection with this. Part of the problem in the oval-shaped breakdown may be a technical difficulty that develops when the generated surface becomes vertical. This would be most expected near the  $v = 0$  plane at the outer edge of the throats. This problem, however, is causally disconnected from the breakdown near the  $u = 0$  plane, so the breakdown cannot wholly be a simple technical flaw in the approach. We are also studying this point, and developing a numerical technique for avoiding this problem, which may be inherent to the Darboux approach.]

Suppose that somehow or another we *were* able to reduce the size of the forbidden region to that of zero area. What would be the implication of such a degenerate embedding shock? It would mean that the embedding diagram is uniquely determined by the initial data on the (approximately) circular outer boundary. That information would propagate inward unambiguously creating the embedding surface in its wake, until it hits the central degenerate shock. Whether the surface generated from one side and that generated from the other meet smoothly at this line is not guaranteed. The degenerate embedding shock would then be a sort of zero measure failure of the local isometric embedding to be global. This leads us to point out that theorems on the existence of global embeddings are notoriously nonexistent. There is no *a priori* reason to suspect that a global embedding of the Misner geometry either does or does not exist.

If a global embedding does not exist, then an attempt to start at an outer circular boundary and propagate inward is doomed to incompleteness. We could, of course, start with inner data, and propagate the embedding diagram outward. But to discuss why we choose not to do this, it is useful at this point to review what we are trying to accomplish with the embedding. To help in the visualization of the physics, the embedding diagram must have the

character of a single throat at large radii, and in some sense must represent the idea of two holes at smaller radii. If a global embedding is impossible, then a diagram started from the central region would be guaranteed, at large radii, to look nothing like the embedding diagram of a single Schwarzschild throat. While there might be some uses to a diagram which represents the inner regions of the Misner geometry, at least for the visualization of initial data for black hole collisions, it would seem much more important to have the desired features at large radii, than in the inner region.

In the discussion above, we have assumed that the forbidden region surrounded by the embedding shock can be reduced to a line, but this may very well not be the case. What if the embedding shocks are unavoidable features that separate the outer region from a nondegenerate inner region? The mathematical parallel between such embedding shocks and the more familiar shocks in gas flow are revealing. In the simplest gas shocks, called “kinematic shocks,” the equation of continuity, along with a relation between propagation velocity and density, leads to a crossing of characteristics[10]. One then argues that the mathematical description is only an approximation to the true physics, and that the approximation breaks down at the shock formation. In principle, one can turn to a more complete description of the physics, such as the Navier-Stokes equation, to arrive at a mathematical formulation without singularities. The simpler approximate mathematics will be adequate on both sides of the shock; the more complete mathematical description will tell us how to “cross” it. That is, how to make the physically appropriate match of the two approximate solutions across the shock.

This sort of strategy is inapplicable to embedding shocks. The Darboux equation is not an approximation; there is not a more complete geometric description that can tell us how to cross the shocks “correctly.” But there is another view of shock-crossing conditions that may be of use. Without reference to a more complete description of the physics, the crossing conditions for gas shocks can be inferred from conservation laws. In the simple case of kinematic shocks, the crossing conditions follow when mass-conservation at the shock is invoked. The resulting solution (without reference to more detailed physics) is then understood to be a “weak” solution—i.e., one which contains singularities, but for which the differential equation is satisfied when it is integrated over any region, including the region of the shock front[10].

What then is the geometric analogy in the case of embeddings? This question is presently being investigated. For now we can only point to

some interesting speculations. We note that for a sufficiently smooth surface, with extrinsic curvature everywhere defined and continuous, there can be no shocks, whether crossed correctly or not. It is interesting, however, to consider an embedding function  $W(u, v)$  in which there are special curves along which the second derivatives of  $W$  are bounded but discontinuous. Such a surface would be smooth (i.e., it would have no creases) but along the special curves, the extrinsic curvature would be discontinuous. At these special curves the directions of the characteristics (which are constrained by the extrinsic curvature) would be multiple-valued. One might imagine that such a surface would be a local isometry to the Misner geometry except along the special curves, and it is tempting to think that this, or some related geometric phenomenon, would represent a weak solution to the embedding problem and the analogy of gas shocks.

For the present, we point out that the embedding shocks do not preclude a partial solution of the embedding problem, which is potentially useful for visual and physical insight. An example is the question of the applicability of perturbation theory to black hole collisions.

If the black holes are initially close together (i.e., if  $\mu_0$  is sufficiently small) the initial geometry *outside the horizon* is nearly spherical. The highly non-spherical geometry inside the horizon does not influence the time evolution of the spacetime outside, so the evolution, and the generation of outgoing gravitational radiation, can be treated as a problem in perturbations of the spherical geometry of a single Schwarzschild throat. An important question is: How small must  $\mu_0$  be for perturbation theory to be valid? As  $\mu_0$  decreases below  $\sim 1.8$  the topology of the horizon on the initial Cauchy hypersurface changes from that of two disjoint spheres (one around each throat) to that of a single 2-sphere surrounding both throats. Only for  $\mu_0$  significantly less than 1.8 will the horizon be reasonably spherical. Yet we know, from comparison with supercomputer evolution of the fully nonlinear equations[1], that perturbation theory works rather well for values of  $\mu_0$  even somewhat larger than 1.8. The explanation would seem to lie in the fact that nonsphericity just outside the horizon disappears down the horizon. In the theory of perturbations of the Schwarzschild geometry[11], outgoing radiation appears to be generated at the peak of the “curvature potential,” located at  $r_{\text{curv}} \approx 3M_{\text{tot}}$ . This radius, roughly, separates the regions in which waves go outward to infinity and go inward towards the hole. A reasonable criterion for applicability of perturbation theory would then seem to lie in the answer to the question:

How nonspherical is the geometry near  $r_{\text{curv}} \approx 3M_{\text{tot}}$ ?

The difficulty in answering this question is that it requires a surface whose sphericity can be evaluated. The horizon is a natural choice but, of course, cannot be located at the peak of the curvature potential. In general, other choices are not gauge invariant, being dependent on coordinate choices. An exception is the coordinate-independent shape of the embedding diagram. We can then ask: How nonspherical is the embedding diagram near  $r_{\text{curv}} \approx 3M_{\text{tot}}$ ? More specifically, we can evaluate the shape of the constant  $W$  contours corresponding to  $r_{\text{curv}} \approx 3M_{\text{tot}}$  and see how they deviate from circles.

In Fig. 6 we present such contours for  $\mu_0 = 1.5, 2, 2.5$ . The error that perturbation theory makes in estimating radiation energy in these three cases is 0, a factor of 2, and a factor of 10, respectively. For each value of  $\mu_0$ , several contours are shown with the properties summarized in Table 1 below. For those contours with  $r := \sqrt{u^2 + v^2} \approx r_{\text{curv}} \approx 3M_{\text{tot}}$  there seems to be a clear correlation between the success of perturbation theory and the spherical (that is, circular) shape of the contours.

$\mu_0 = 1.5$			$\mu_0 = 2$			$\mu_0 = 2.5$		
$r_{\text{max}}$	$r_{\text{min}}$	$\Delta r/r_{\text{max}}^a$	$r_{\text{max}}$	$r_{\text{min}}$	$\Delta r/r_{\text{max}}$	$r_{\text{max}}$	$r_{\text{min}}$	$\Delta r/r_{\text{max}}$
2.50	2.36	.056	2.77	2.38	.141	3.05	2.45	.197 <sup>b</sup>
2.94	2.86	.027	3.12	2.87	.080	3.56	2.91	.183
3.60	3.56	.011	3.72	3.57	.040	4.02	3.61	.102
4.48	4.45	.007	4.56	4.47	.020	4.75	4.52	.048

<sup>a</sup>  $\Delta r \equiv r_{\text{max}} - r_{\text{min}}$       <sup>b</sup> incomplete curve

Table 1: Noncircularity of constant  $W$  contours

## Acknowledgments

We thank Andrejs Treibergs for useful suggestions and extensive discussions of mathematical issues in connection with embeddings. The argument we gave in Sec. 4 involving the Poincaré index theorem arose during one of our discussions. We also thank Ed Seidel of NCSA for valuable suggestions, and David Bernstein of the University of New England, Australia, for discussions of his work on the embedding problem. JDR thanks Carsten Gundlach for



help with the numerical code. The work reported here was supported by grant NSF-PHY-92-07225, and by research funds of the University of Utah.

## Appendix

### A.1 Coefficients of the Darboux equation

The coefficients  $\mathcal{A}, \mathcal{B}, \dots, \mathcal{E}$  of the Darboux equation are

$$\mathcal{A} = -4(EG - F^2) \quad (40)$$

$$\mathcal{B} = +2p(2GF_{,y} - GG_{,x} - FG_{,y}) + 2q(-2FF_{,y} + FG_{,x} + EG_{,y}) \quad (41)$$

$$\mathcal{C} = +4p(FG_{,x} - GE_{,y}) + 4q(FE_{,y} - EG_{,x}) \quad (42)$$

$$\mathcal{D} = -2p(2FF_{,x} - GE_{,x} - FE_{,y}) - 2q(-2EF_{,x} + FE_{,x} + EE_{,y}) \quad (43)$$

$$\begin{aligned} \mathcal{E} = & +(E - p^2)(E_{,y}G_{,y} - 2F_{,x}G_{,y} + G_{,x}^2) \\ & +(F - pq)(E_{,x}G_{,y} - E_{,y}G_{,x} - 2E_{,y}F_{,y} - 2F_{,x}G_{,x} + 4F_{,x}F_{,y}) \\ & +(G - q^2)(E_{,x}G_{,x} - 2E_{,x}F_{,y} + E_{,y}^2) \\ & +2((E - p^2)(G - q^2) - (F - pq)^2)(2F_{,xy} - E_{,yy} - G_{,xx}). \end{aligned} \quad (44)$$

Here  $W(x, y)$  is one of the three embedding functions  $(U, V, W)$ , and  $p$  and  $q$  are shorthand notations for the partial derivatives  $W_{,x}$  and  $W_{,y}$ . The functions  $E, F, G$  are the components of the 2-geometry that is to be embedded.

### A.2 Gaussian curvature

The Gaussian curvature  $K$  of a 2-geometry having components  $E, F, G$  is given by

$$\begin{aligned} K = & \left[ 2(EG - F^2)(-E_{,yy} + 2F_{,xy} - G_{,xx}) \right. \\ & + E(G_{,x}^2 - 2F_{,x}G_{,y} + E_{,y}G_{,y}) \\ & + F(E_{,x}G_{,y} - E_{,y}G_{,x} + 4F_{,x}F_{,y} - 2E_{,y}F_{,y} - 2F_{,x}G_{,x}) \\ & \left. + G(E_{,y}^2 - 2E_{,x}F_{,y} + E_{,x}G_{,x}) \right] / 4(EG - F^2)^2. \end{aligned} \quad (45)$$

It is an intrinsic property of the 2-geometry, independent of any embedding.

### A.3 Unit normal

The unit normal  $\vec{n}$  to a surface depends explicitly on the embedding functions  $\vec{f} := (U, V, W)$ . Up to a normalization factor, it is given by the usual Euclidean 3-space vector product of  $\vec{f}_{,x}$  and  $\vec{f}_{,y}$ . When adjusted to be of unit length and reexpressed using (3)-(5), the unit normal can be written as

$$\vec{n} = \frac{\vec{f}_{,x} \times \vec{f}_{,y}}{\sqrt{EG - F^2}}. \quad (46)$$

The  $(u, v, w)$ -components of  $\vec{n}$  are

$$n^1 = \frac{(V_{,x}W_{,y} - V_{,y}W_{,x})}{\sqrt{EG - F^2}} \quad (47)$$

$$n^2 = \frac{(W_{,x}U_{,y} - W_{,y}U_{,x})}{\sqrt{EG - F^2}} \quad (48)$$

$$n^3 = \frac{(U_{,x}V_{,y} - U_{,y}V_{,x})}{\sqrt{EG - F^2}}. \quad (49)$$

### A.4 Extrinsic Curvature

The extrinsic curvature  $\mathbf{K}$  is a tensor on the 2-geometry that describes the shape of the embedded surface and depends on the embedding functions  $\vec{f} = (U, V, W)$ . In terms of  $\vec{f}$  and the unit normal  $\vec{n}$ , its  $(x, y)$ -components can be written as

$$K_{11} = \vec{f}_{,xx} \cdot \vec{n} \quad (50)$$

$$K_{12} = \vec{f}_{,xy} \cdot \vec{n} \quad (51)$$

$$K_{22} = \vec{f}_{,yy} \cdot \vec{n}. \quad (52)$$

Here  $\cdot$  denotes the usual Euclidean 3-space dot product of two vectors.

### A.5 The hyperbolic Monge-Ampère equation as a characteristic system

We outline here how the hyperbolic Monge-Ampère equation can be written as a characteristic system of quasilinear, first-order PDEs for the unknowns  $(x, y, W, p, q)$ . More details can be found in the text by Courant and Hilbert[5].

We start with the Monge-Ampère equation

$$Q := \mathcal{A}(rt - s^2) + \mathcal{B}r + \mathcal{C}s + Dt + \mathcal{E} = 0. \quad (53)$$

This is a nonlinear, second-order PDE for a single unknown function  $W(x, y)$ . The only requirement on the coefficients  $\mathcal{A}, \mathcal{B}, \dots, \mathcal{E}$  is that they be independent of the second partial derivatives  $r := W_{,xx}$ ,  $s := W_{,xy}$ ,  $t := W_{,yy}$ . They can depend nonlinearly on  $x, y$ , and  $W$ , and on the first partial derivatives  $p := W_{,x}$  and  $q := W_{,y}$ .

Assume that the equation is hyperbolic, so that

$$\Delta := Q_{,s}^2 - 4Q_{,r}Q_{,t} > 0. \quad (54)$$

In terms of the coefficients  $\mathcal{A}, \mathcal{B}, \dots, \mathcal{E}$ , we have

$$\begin{aligned} \Delta &= (\mathcal{C} - 2\mathcal{A}s)^2 - 4(\mathcal{B} + \mathcal{A}t)(\mathcal{D} + \mathcal{A}r) \\ &= \mathcal{C}^2 - 4\mathcal{B}\mathcal{D} + 4\mathcal{A}\mathcal{E}. \end{aligned} \quad (55)$$

Here we used (53) to eliminate  $r, s, t$  to obtain the second equality. The first equality is actually an important “identity” that we will use later on in our analysis. We choose to write this identity in the form

$$\frac{\mathcal{C} - 2\mathcal{A}s + \delta}{2(\mathcal{B} + \mathcal{A}t)} = \frac{2(\mathcal{D} + \mathcal{A}r)}{\mathcal{C} - 2\mathcal{A}s - \delta} \quad (56)$$

where

$$\delta := \sqrt{\Delta} = \sqrt{\mathcal{C}^2 - 4\mathcal{B}\mathcal{D} + 4\mathcal{A}\mathcal{E}}. \quad (57)$$

Since equation (53) was assumed to be hyperbolic,  $\delta$  is real and is taken to be positive.

We next write down the solutions to the characteristic equation

$$Q_{,r} \left( \frac{dy}{dx} \right)^2 - Q_{,s} \left( \frac{dy}{dx} \right) + Q_{,t} = 0. \quad (58)$$

In terms of the coefficients  $\mathcal{A}, \mathcal{B}, \dots, \mathcal{E}$ , the solutions are

$$\left( \frac{dy}{dx} \right)_{\pm} = \frac{\mathcal{C} - 2\mathcal{A}s \pm \delta}{2(\mathcal{B} + \mathcal{A}t)}. \quad (59)$$

Since  $\delta > 0$ , there exist two distinct characteristic directions at each point. We can integrate along these directions to obtain the characteristic curves,

which we label by two parameters  $\alpha$  and  $\beta$ . If we choose  $\alpha$  and  $\beta$  to be constant along the curves having the directions  $(dy/dx)_+$  and  $(dy/dx)_-$ , respectively, then

$$\left(\frac{dy}{dx}\right)_+ = \frac{y_{,\beta}}{x_{,\beta}} \quad \text{and} \quad \left(\frac{dy}{dx}\right)_- = \frac{y_{,\alpha}}{x_{,\alpha}}. \quad (60)$$

Here  $x$  and  $y$  are to be thought of as unknown functions of the characteristic coordinates  $(\alpha, \beta)$ . The switch from  $(x, y)$  to  $(\alpha, \beta)$  as independent variables is allowed wherever the Jacobian of the transformation  $x_{,\alpha}y_{,\beta} - x_{,\beta}y_{,\alpha} \neq 0$ .

Using (59) and (60), we obtain two equations

$$(\mathcal{B} + \mathcal{A}t)y_{,\alpha} - \frac{1}{2}(\mathcal{C} - 2\mathcal{A}s - \delta)x_{,\alpha} = 0 \quad (61)$$

$$(\mathcal{B} + \mathcal{A}t)y_{,\beta} - \frac{1}{2}(\mathcal{C} - 2\mathcal{A}s + \delta)x_{,\beta} = 0. \quad (62)$$

These two equations together with the identity (56) give us two additional equations

$$\frac{1}{2}(\mathcal{C} - 2\mathcal{A}s + \delta)y_{,\alpha} - (\mathcal{D} + \mathcal{A}r)x_{,\alpha} = 0 \quad (63)$$

$$\frac{1}{2}(\mathcal{C} - 2\mathcal{A}s - \delta)y_{,\beta} - (\mathcal{D} + \mathcal{A}r)x_{,\beta} = 0. \quad (64)$$

These are four first-order PDEs in the unknowns  $x, y$ . But we must still deal with the unknowns  $W, p, q, r, s, t$ .

To this end, consider the first- and second-order strip equations. They are

$$W_{,\alpha} = p x_{,\alpha} + q y_{,\alpha} \quad (65)$$

$$W_{,\beta} = p x_{,\beta} + q y_{,\beta} \quad (66)$$

and

$$p_{,\alpha} = r x_{,\alpha} + s y_{,\alpha} \quad (67)$$

$$p_{,\beta} = r x_{,\beta} + s y_{,\beta} \quad (68)$$

$$q_{,\alpha} = s x_{,\alpha} + t y_{,\alpha} \quad (69)$$

$$q_{,\beta} = s x_{,\beta} + t y_{,\beta} \quad (70)$$

respectively. These equations are needed to guarantee that

$$p = W_{,x} \quad q = W_{,y} \quad r = W_{,xx} \quad s = W_{,xy} \quad t = W_{,yy}. \quad (71)$$

By substituting the second-order strip equations into (61)-(64) we can eliminate the dependence on  $r, s, t$ , and write the results as

$$\mathcal{B} y_{,\alpha} + \mathcal{A} q_{,\alpha} - \frac{1}{2}(\mathcal{C} - \delta) x_{,\alpha} = 0 \quad (72)$$

$$\mathcal{B} y_{,\beta} + \mathcal{A} q_{,\beta} - \frac{1}{2}(\mathcal{C} + \delta) x_{,\beta} = 0 \quad (73)$$

$$\frac{1}{2}(\mathcal{C} + \delta) y_{,\alpha} - \mathcal{D} x_{,\alpha} - \mathcal{A} p_{,\alpha} = 0 \quad (74)$$

$$\frac{1}{2}(\mathcal{C} - \delta) y_{,\beta} - \mathcal{D} x_{,\beta} - \mathcal{A} p_{,\beta} = 0. \quad (75)$$

These are four quasilinear, first-order PDEs in the five unknowns  $(x, y, W, p, q)$ . (Quasilinear in the sense that the equations depend linearly on the first partial derivatives of  $(x, y, W, p, q)$ .) In order to complete the system, we need an additional independent equation. We choose this to be the first-order strip equation

$$W_{,\alpha} - p x_{,\alpha} - q y_{,\alpha} = 0. \quad (76)$$

The above five equations are equations (18)-(22) in the main text. This is the desired result.

## A.6 Determining $U$ and $V$ via quadratures

After  $W$  has been found as a function of  $(x, y)$  we must still determine the remaining embedding functions  $U(x, y), V(x, y)$ . We could in principle solve (3)-(5) directly, but there is a simpler approach, again due to Darboux, that we use and outline here. (For further discussion, see [6].)

Consider a general, positive-definite, 2-dimensional line element

$$ds^2 = f_{11} dx^2 + 2f_{12} dx dy + f_{22} dy^2 \quad (77)$$

with metric components denoted by  $f_{ij}$ . Then the Gaussian curvature  $K$  of (77) can be written as

$$\sqrt{f} K = (B_{,x} - A_{,y}) \quad (78)$$

where  $f := f_{11}f_{22} - (f_{12})^2$  is the determinant of the matrix of components  $f_{ij}$  and

$$A = \frac{1}{2\sqrt{f}} \left[ \left( \frac{f_{12}}{f_{11}} \right) f_{11,x} + f_{11,y} - f_{12,x} \right] \quad (79)$$

$$B = \frac{1}{2\sqrt{f}} \left[ \left( \frac{f_{12}}{f_{11}} \right) f_{11,y} - f_{22,x} + f_{12,y} \right]. \quad (80)$$

Using (78) and Stoke's theorem, we can write

$$\int_{\Omega} \sqrt{f} K dx dy = \oint_{\partial\Omega} (A dx + B dy), \quad (81)$$

where the integral on the left hand side of the above equation is taken over some simply-connected 2-dimensional region  $\Omega$ . The integral on the right hand side is around the closed 1-dimensional boundary  $\partial\Omega$ .

If  $K = 0$  at every point  $(x, y)$ , the right hand side of (81) vanishes for all closed curves  $\partial\Omega$ . This means that there exists a function  $\vartheta(x, y)$  such that

$$\vartheta_{,x} = A \quad \text{and} \quad \vartheta_{,y} = B. \quad (82)$$

One can then integrate equations (82) directly to obtain an expression for  $\vartheta$  in terms of the components  $f_{ij}$ . The solution is determined up to an overall additive constant. Moreover, using (82) and the definitions (79) and (80) of  $A$  and  $B$ , one can show that

$$\left( -\sqrt{f_{11}} \sin \vartheta \right)_{,y} = \left( -\frac{f_{12}}{\sqrt{f_{11}}} \sin \vartheta + \frac{\sqrt{f}}{\sqrt{f_{11}}} \cos \vartheta \right)_{,x} \quad (83)$$

$$\left( +\sqrt{f_{11}} \cos \vartheta \right)_{,y} = \left( +\frac{f_{12}}{\sqrt{f_{11}}} \cos \vartheta + \frac{\sqrt{f}}{\sqrt{f_{11}}} \sin \vartheta \right)_{,x}. \quad (84)$$

This means that there exist functions  $U(x, y)$ ,  $V(x, y)$  such that

$$U_{,x} = -\sqrt{f_{11}} \sin \vartheta \quad (85)$$

$$U_{,y} = -\frac{f_{12}}{\sqrt{f_{11}}} \sin \vartheta + \frac{\sqrt{f}}{\sqrt{f_{11}}} \cos \vartheta \quad (86)$$

$$V_{,x} = +\sqrt{f_{11}} \cos \vartheta \quad (87)$$

$$V_{,y} = +\frac{f_{12}}{\sqrt{f_{11}}} \cos \vartheta + \frac{\sqrt{f}}{\sqrt{f_{11}}} \sin \vartheta. \quad (88)$$

These equations can also be integrated directly, allowing us to obtain expressions for  $U, V$  in terms of the components  $f_{ij}$ . The solutions for  $U, V$  are determined up to overall additive constants.

The freedom in choosing the additive constants for  $\vartheta, U, V$  corresponds to the freedom of performing a 2-dimensional Euclidean motion of the plane. Such a motion preserves the form of the line element  $du^2 + dv^2$ . The additive constant for  $\vartheta$  corresponds to a rigid rotation of the plane about the origin. The additive constants for  $U, V$  correspond to a translation.

Given the above results, we now specialize to the case of the flat 2-dimensional line element (7). This line element has components

$$f_{11} = E - p^2 \tag{89}$$

$$f_{12} = F - pq \tag{90}$$

$$f_{22} = G - q^2 \tag{91}$$

where  $p = W_{,x}$  and  $q = W_{,y}$ . The solutions for  $\vartheta, U, V$  that we find by integrating (82) and (85)-(88) (using the above  $f_{ij}$ ) complete the embedding.

## A.7 Gaussian curvature of the Misner 2-geometry

We start with the Misner 2-geometry

$$ds^2 = a^2 \varphi_{\text{Misner}}^4 [d\mu^2 + d\eta^2] \tag{92}$$

written in terms of the coordinates  $(\mu, \eta)$ . To simplify the notation in what follows, we will drop the ‘‘Misner’’ subscript from  $\varphi_{\text{Misner}}$  and define

$$[n] := \cosh(\mu + 2n\mu_0) - \cos \eta. \tag{93}$$

Then

$$\varphi := \varphi_{\text{Misner}} = \sum_{n=-\infty}^{\infty} [n]^{-1/2}. \tag{94}$$

Our goal is to calculate the Gaussian curvature  $K$  of (92), and to write it in a form which is manifestly everywhere-negative. If we take  $(\mu, \eta)$  as our coordinates  $(x, y)$  then

$$E = G = a^2 \varphi^4 \quad \text{and} \quad F = 0 \tag{95}$$

are the components of the Misner 2-geometry. For  $E = G$ ,  $F = 0$ , the expression (45) for the Gaussian curvature simplifies considerably:

$$K = -\frac{1}{2} E^{-1} [(\ln E)_{,xx} + (\ln E)_{,yy}] . \quad (96)$$

This is just minus one-half times the covariant Laplacian of  $\ln E$ . For  $E = a^2 \varphi^4$ , we have

$$K = -2 a^{-2} \varphi^{-4} [(\ln \varphi)_{,\mu\mu} + (\ln \varphi)_{,\eta\eta}] . \quad (97)$$

This is what we must evaluate.

We begin by calculating the first and second partial derivatives of  $\varphi$ . They are

$$\varphi_{,\mu} = \sum_{n=-\infty}^{\infty} -\frac{1}{2} [n]^{-3/2} \sinh(\mu + 2n\mu_0) \quad (98)$$

$$\varphi_{,\eta} = \sum_{n=-\infty}^{\infty} -\frac{1}{2} [n]^{-3/2} \sin \eta \quad (99)$$

$$\begin{aligned} \varphi_{,\mu\mu} = \sum_{n=-\infty}^{\infty} \left( -\frac{1}{2} [n]^{-3/2} \cosh(\mu + 2n\mu_0) \right. \\ \left. + \frac{3}{4} [n]^{-5/2} \sinh^2(\mu + 2n\mu_0) \right) \end{aligned} \quad (100)$$

$$\varphi_{,\eta\eta} = \sum_{n=-\infty}^{\infty} \left( -\frac{1}{2} [n]^{-3/2} \cos \eta + \frac{3}{4} [n]^{-5/2} \sin^2 \eta \right) . \quad (101)$$

Since

$$(\ln \varphi)_{,\mu\mu} + (\ln \varphi)_{,\eta\eta} = \varphi^{-2} \left[ \varphi \varphi_{,\mu\mu} + \varphi \varphi_{,\eta\eta} - (\varphi_{,\mu})^2 - (\varphi_{,\eta})^2 \right] , \quad (102)$$

it is also convenient to evaluate

$$\begin{aligned} & \varphi \varphi_{,\mu\mu} + \varphi \varphi_{,\eta\eta} \\ &= \frac{1}{4} \sum_{m=-\infty}^{\infty} \sum_{n=-\infty}^{\infty} \frac{\cosh(\mu + 2m\mu_0) \cosh(\mu + 2n\mu_0) - \cos^2 \eta}{[m]^{3/2} [n]^{3/2}} \end{aligned} \quad (103)$$

$$\begin{aligned} & (\varphi_{,\mu})^2 + (\varphi_{,\eta})^2 \\ &= \frac{1}{4} \sum_{m=-\infty}^{\infty} \sum_{n=-\infty}^{\infty} \frac{\sinh(\mu + 2m\mu_0) \sinh(\mu + 2n\mu_0) + \sin^2 \eta}{[m]^{3/2} [n]^{3/2}} . \end{aligned} \quad (104)$$



Combining (102), (103), and (104) we see that

$$\begin{aligned}
& (\ln \varphi)_{,\mu\mu} + (\ln \varphi)_{,\eta\eta} \\
&= \varphi^{-2} \left[ \varphi \varphi_{,\mu\mu} + \varphi \varphi_{,\eta\eta} - (\varphi_{,\mu})^2 - (\varphi_{,\eta})^2 \right] \\
&= \frac{1}{4} \varphi^{-2} \sum_{m=-\infty}^{\infty} \sum_{n=-\infty}^{\infty} \frac{\cosh(2\mu_0(m-n)) - 1}{[m]^{3/2} [n]^{3/2}}. \tag{105}
\end{aligned}$$

From this we get the final result

$$K = -\frac{1}{2} a^{-2} \varphi^{-6} \sum_{m=-\infty}^{\infty} \sum_{n=-\infty}^{\infty} \frac{\cosh(2\mu_0(m-n)) - 1}{[m]^{3/2} [n]^{3/2}}. \tag{106}$$

This is the manifestly negative-definite expression for the Gaussian curvature given in the main text.

One may rightfully worry about those places where

$$[n] := \cosh(\mu + 2n\mu_0) - \cos \eta = 0. \tag{107}$$

When this happens,  $\varphi = \sum [n]^{-1/2} \rightarrow \infty$  and  $K \rightarrow 0$ . This occurs only if

$$\eta = 0 \quad \text{and} \quad \mu + 2n\mu_0 = 0 \tag{108}$$

where  $n$  is an integer. For  $-\mu_0 \leq \mu \leq \mu_0$ , we see that the second equality holds only if  $\mu = 0$  and  $n = 0$ . Thus,  $[n] = 0$  if and only if  $(\mu, \eta) = (0, 0)$ . This is the ‘‘point’’ at spatial infinity, and there we expect the 2-geometry corresponding to the Misner data to be flat.

## References

- [1] Anninos P, Hobill D, Seidel E, Smarr L, and Suen W-M 1993 “The Collision of Two Black Holes” *Phys. Rev. Lett.* **71** 2851-2854
- [2] Price R H and Pullin J 1994 “Colliding Black Holes: The Close Limit” *Phys. Rev. Lett.* **72** 3297-3300; Abrahams A M and Cook G B 1994 “Collisions of Boosted Black Holes: Perturbation Theory Prediction of Gravitational Radiation” *Phys. Rev.* **D50** R2364-2367
- [3] Misner C W 1960 “Wormhole Initial Conditions” *Phys. Rev.* **118** 1110-1111
- [4] Spivak M 1975 *A Comprehensive Introduction to Differential Geometry, Volume 5* (Boston: Publish or Perish) Chap 11
- [5] Courant R and Hilbert D 1962 *Methods of Mathematical Physics, Volume II: Partial Differential Equations* (New York: Interscience) Appendix 1 to Chap 5
- [6] Hartman P and Wintner A 1951 “Gaussian Curvature and Local Embedding” *Am. Jour. of Math.* **73** 876-884
- [7] Poznyak É G and Shikin E V 1976 “Surfaces of Negative Curvature” *Jour. of Soviet Math.* **5** 865-887
- [8] Bernstein D 1994 “An Iterative Scheme for Computing Isometric Embedding Diagrams for use in Numerical Relativity Calculations” University of New England, Australia Preprint
- [9] Hsiung C-C 1981 *A First Course in Differential Geometry* (New York: Wiley) pp 264-267
- [10] Whitham G B 1974 *Linear and Nonlinear Waves* (New York: Wiley) Chap 2
- [11] Sun Y and Price R H 1990 “Excitation of Schwarzschild Quasinormal Modes by Collapse” *Phys. Rev.* **D41** 2492-2506

## Figure Captions

Fig. 1: The net of characteristics propagating inward from the  $R = \text{const}$  initial value surface for  $\mu_0 = 1, 2, 3$ .

Fig. 2: The principal directions of the extrinsic curvature and the characteristic directions near the center.

Fig. 3: The computed crossing of two characteristics of the same family for  $\mu_0 = 6$ .

Fig. 4: Shapes of 3-dimensional embedding diagrams when viewed along the  $v$  axis for  $\mu_0 = 1, 3$ .

Fig. 5: Perspective view of the (incomplete) embedding diagram for  $\mu_0 = 3$ .

Fig. 6: Constant  $W$  contours of the embedding diagrams for  $\mu_0 = 1.5, 2, 2.5$ .

This figure "fig1-1.png" is available in "png" format from:

<http://arxiv.org/ps/gr-qc/9409047v1>

Figure 1a

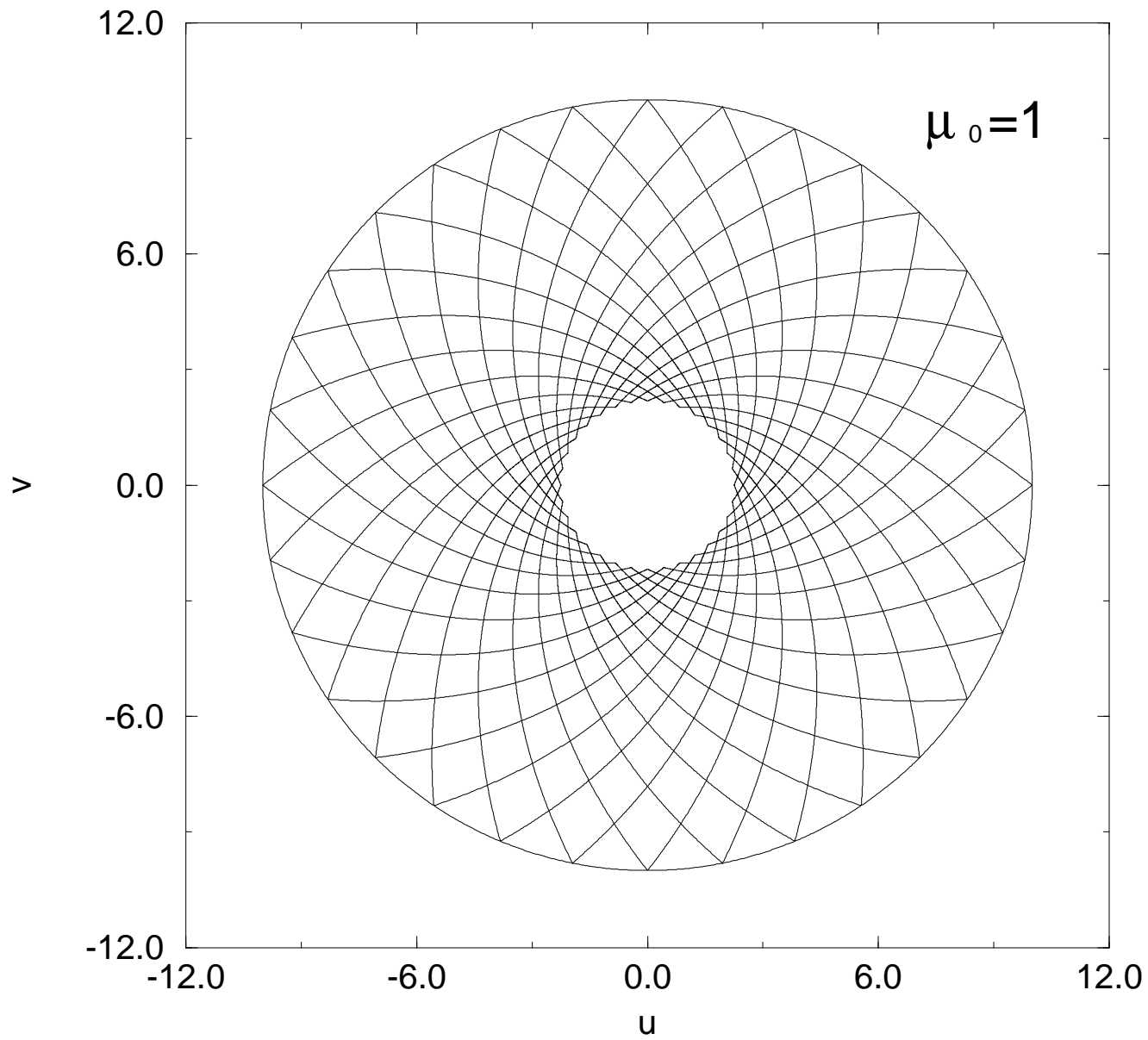


Figure 1b

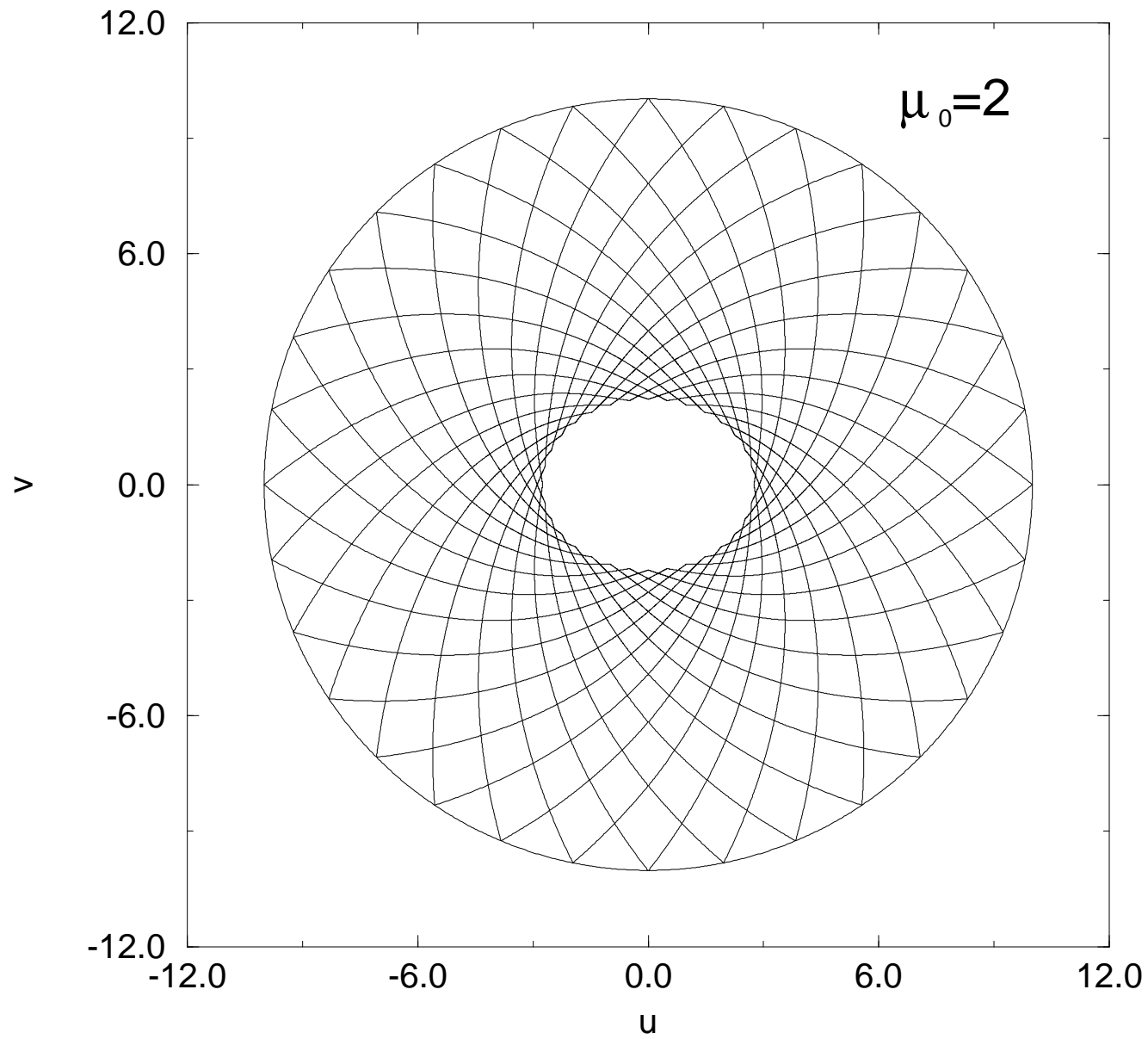
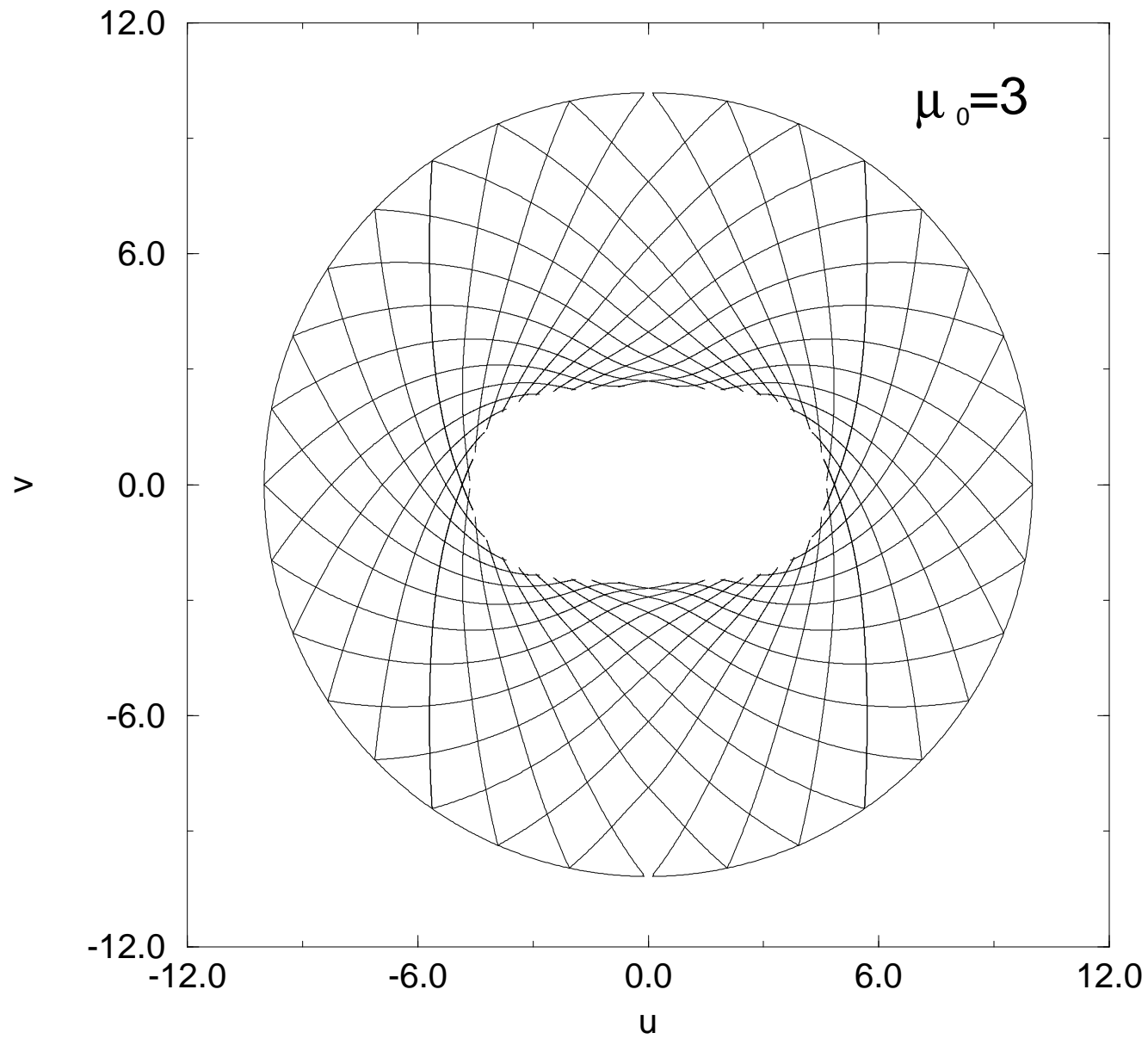


Figure 1c



This figure "fig1-2.png" is available in "png" format from:

<http://arxiv.org/ps/gr-qc/9409047v1>



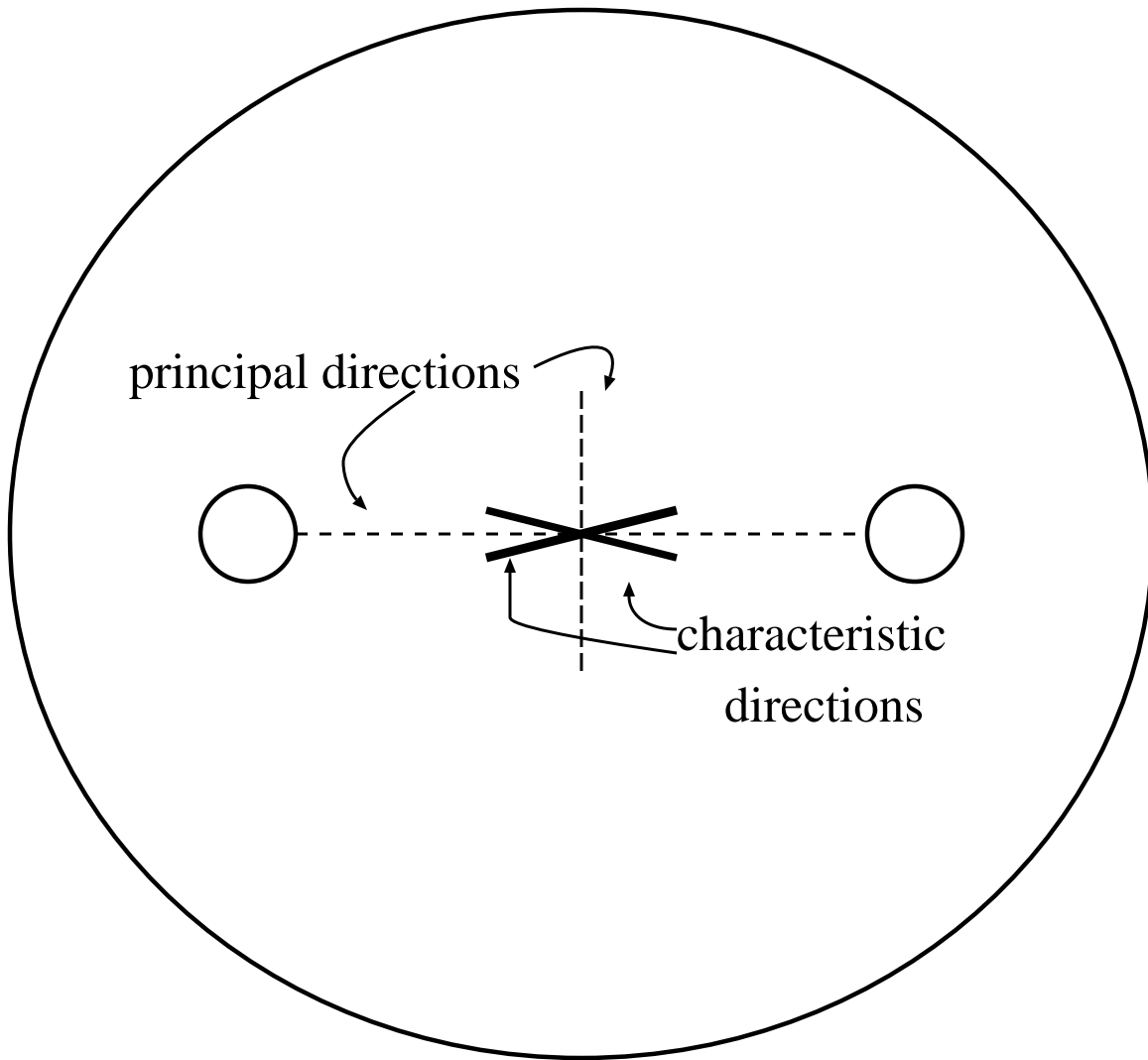
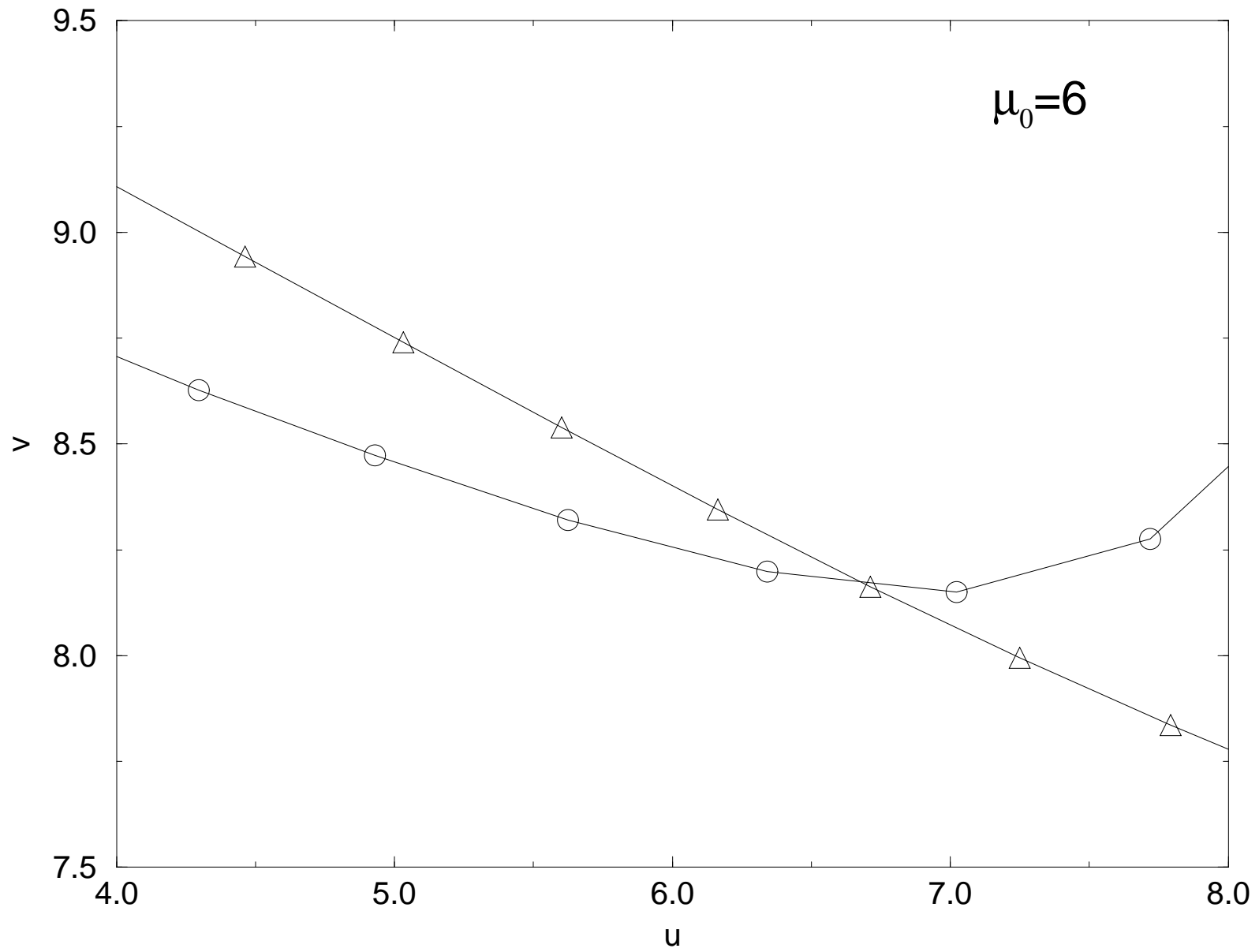


FIGURE 2

This figure "fig1-3.png" is available in "png" format from:

<http://arxiv.org/ps/gr-qc/9409047v1>

Figure 3



This figure "fig1-4.png" is available in "png" format from:

<http://arxiv.org/ps/gr-qc/9409047v1>

Figure 4a

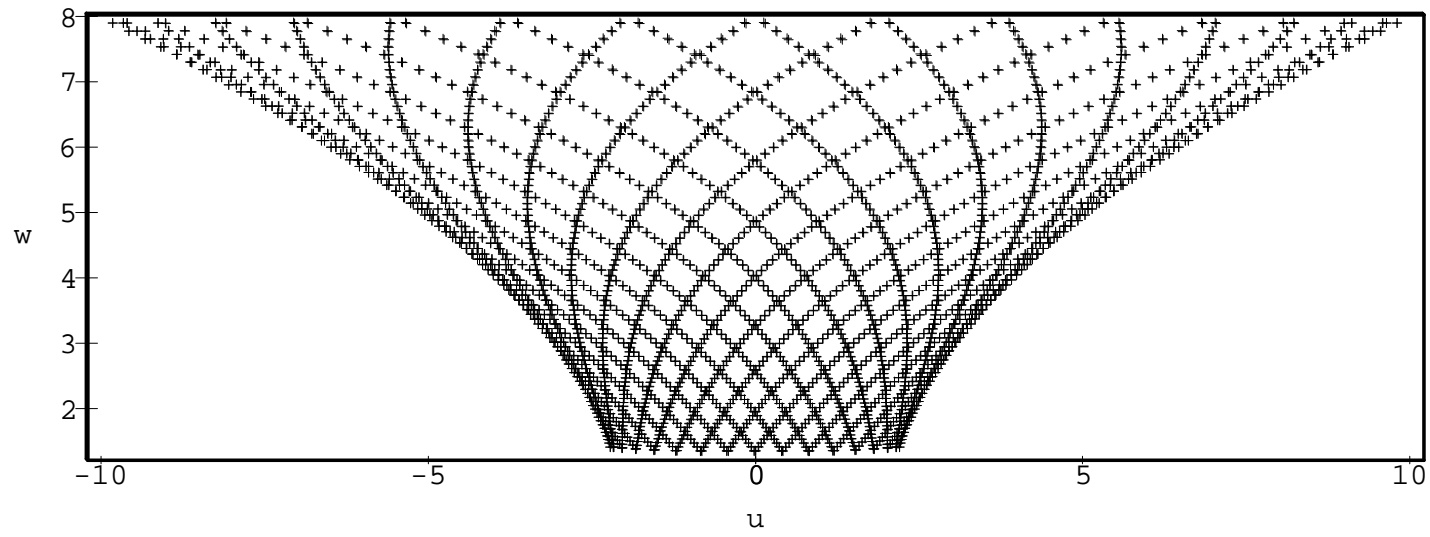
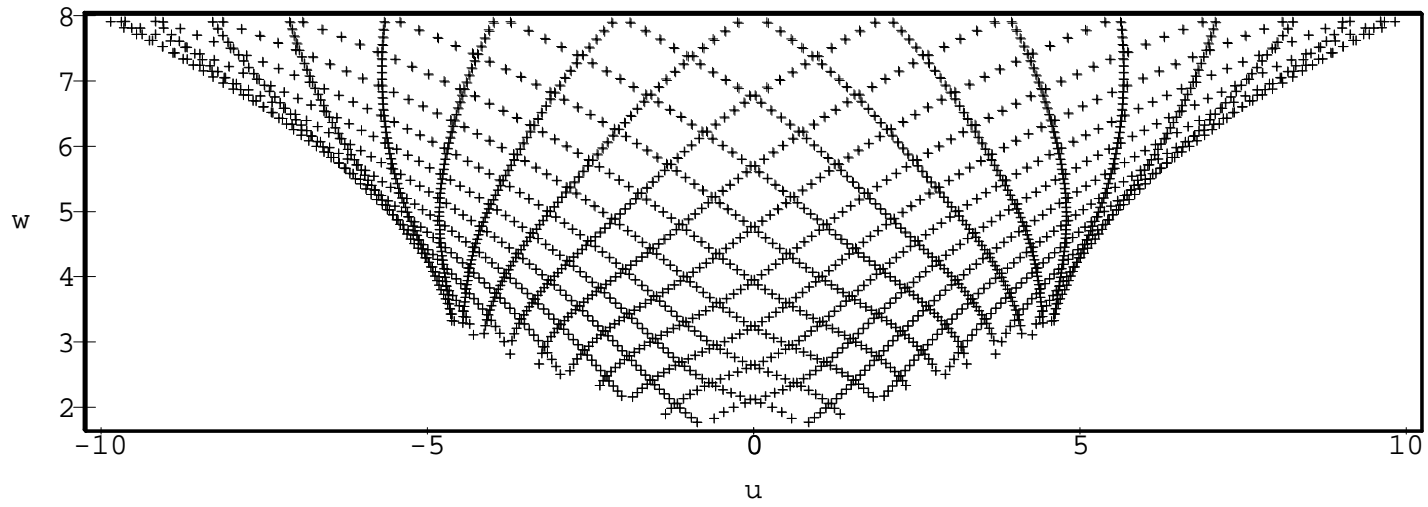


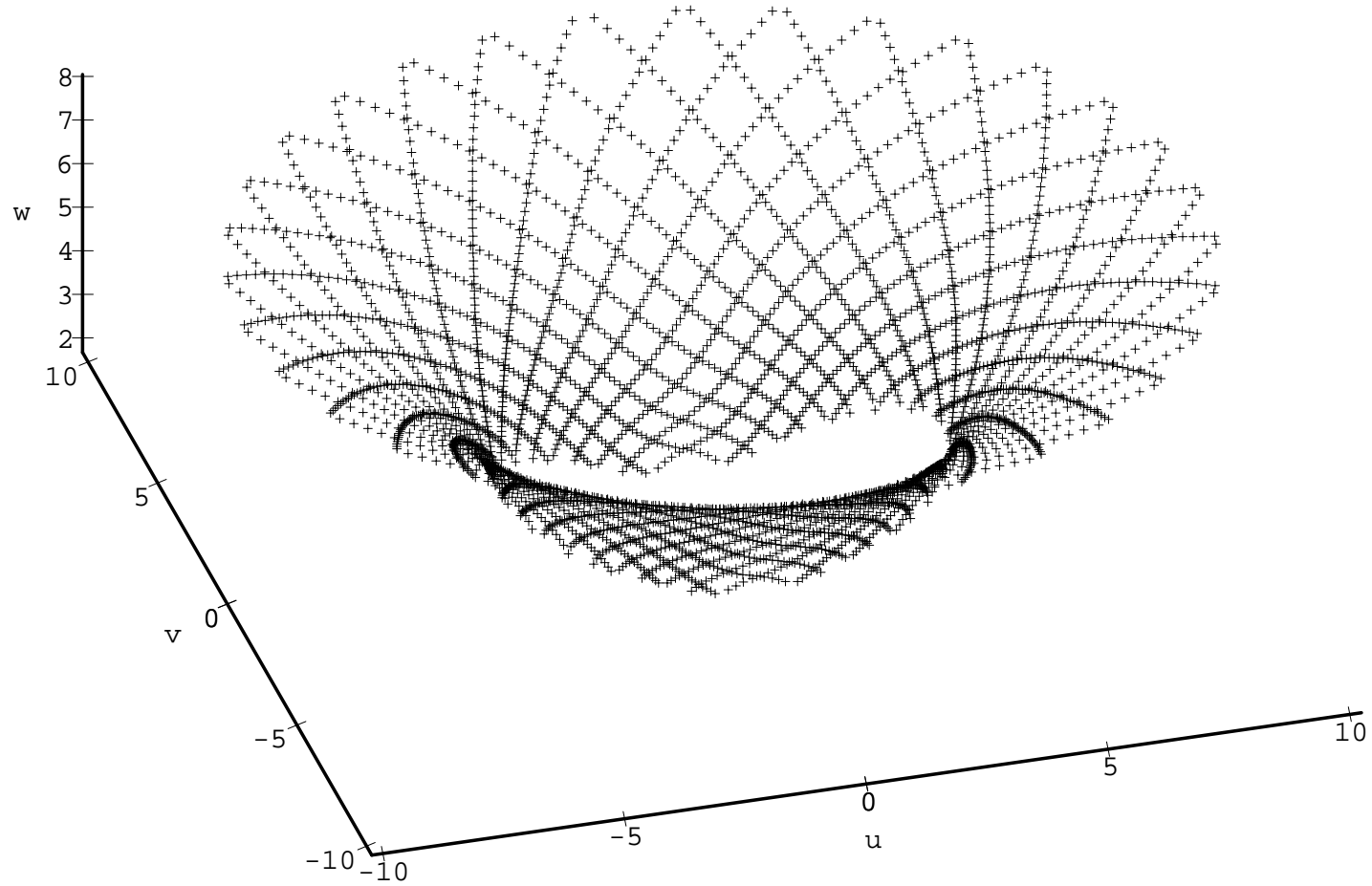
Figure 4b



This figure "fig1-5.png" is available in "png" format from:

<http://arxiv.org/ps/gr-qc/9409047v1>

Figure 5





This figure "fig1-6.png" is available in "png" format from:

<http://arxiv.org/ps/gr-qc/9409047v1>

Figure 6a

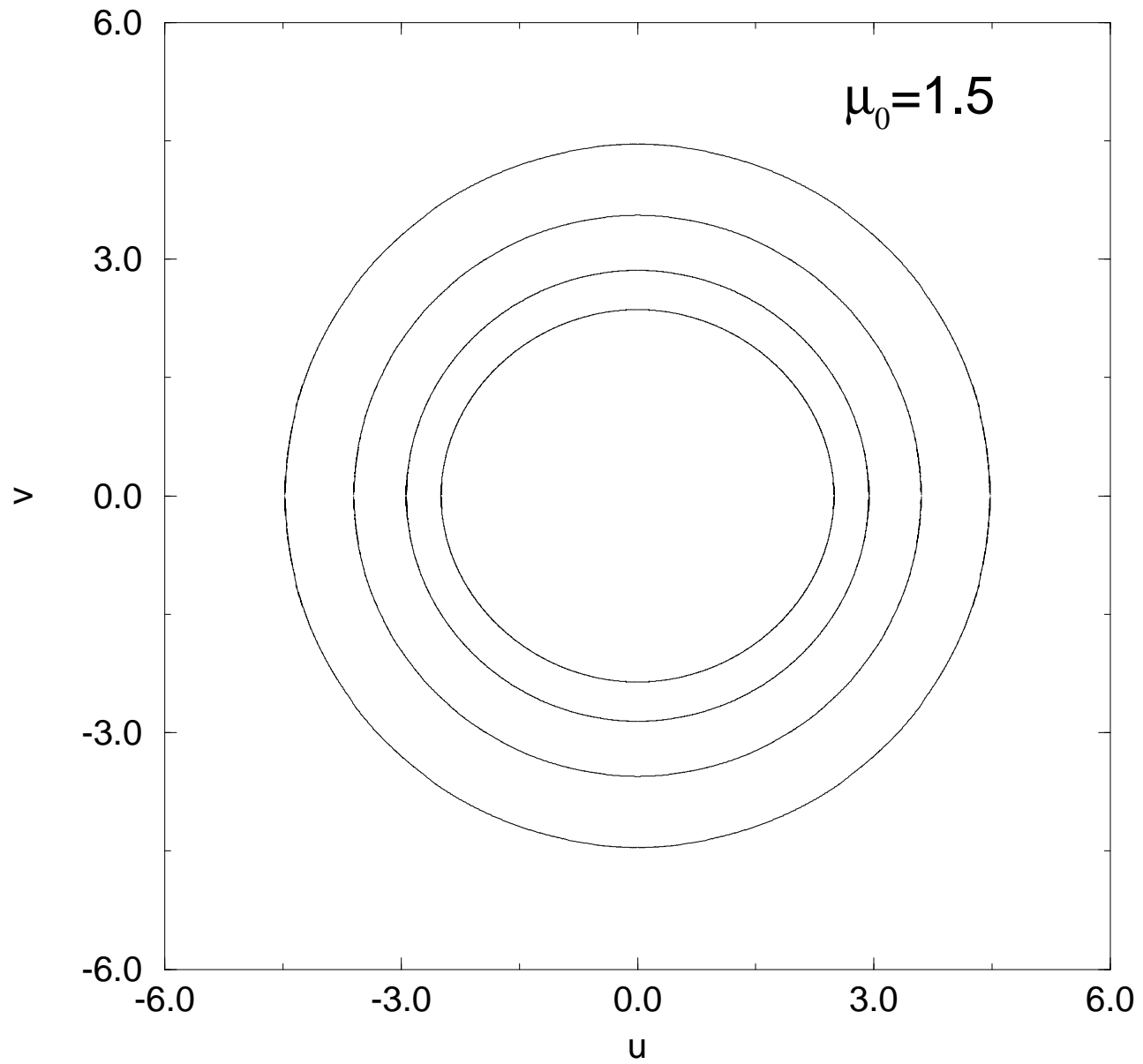


Figure 6b

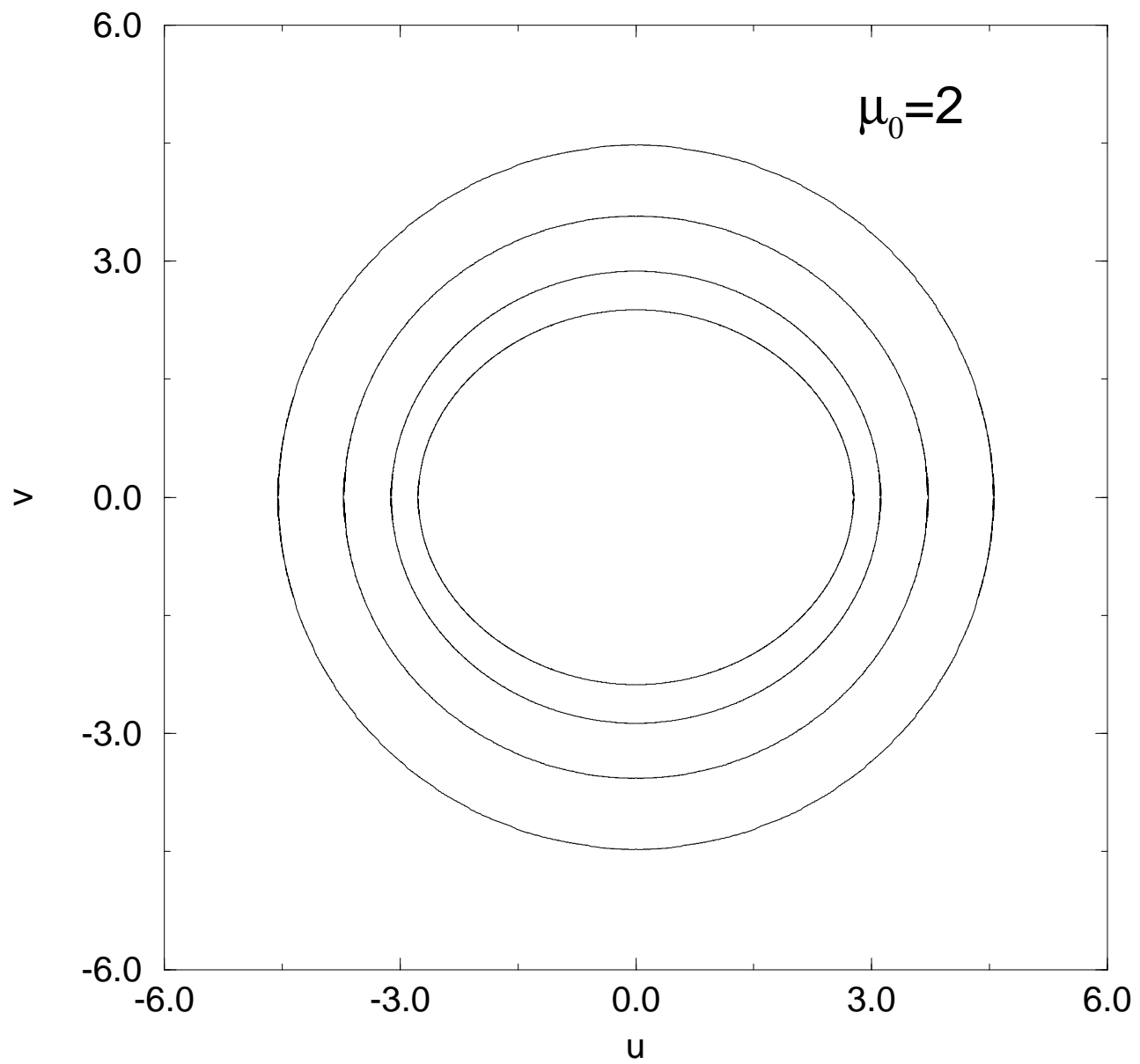
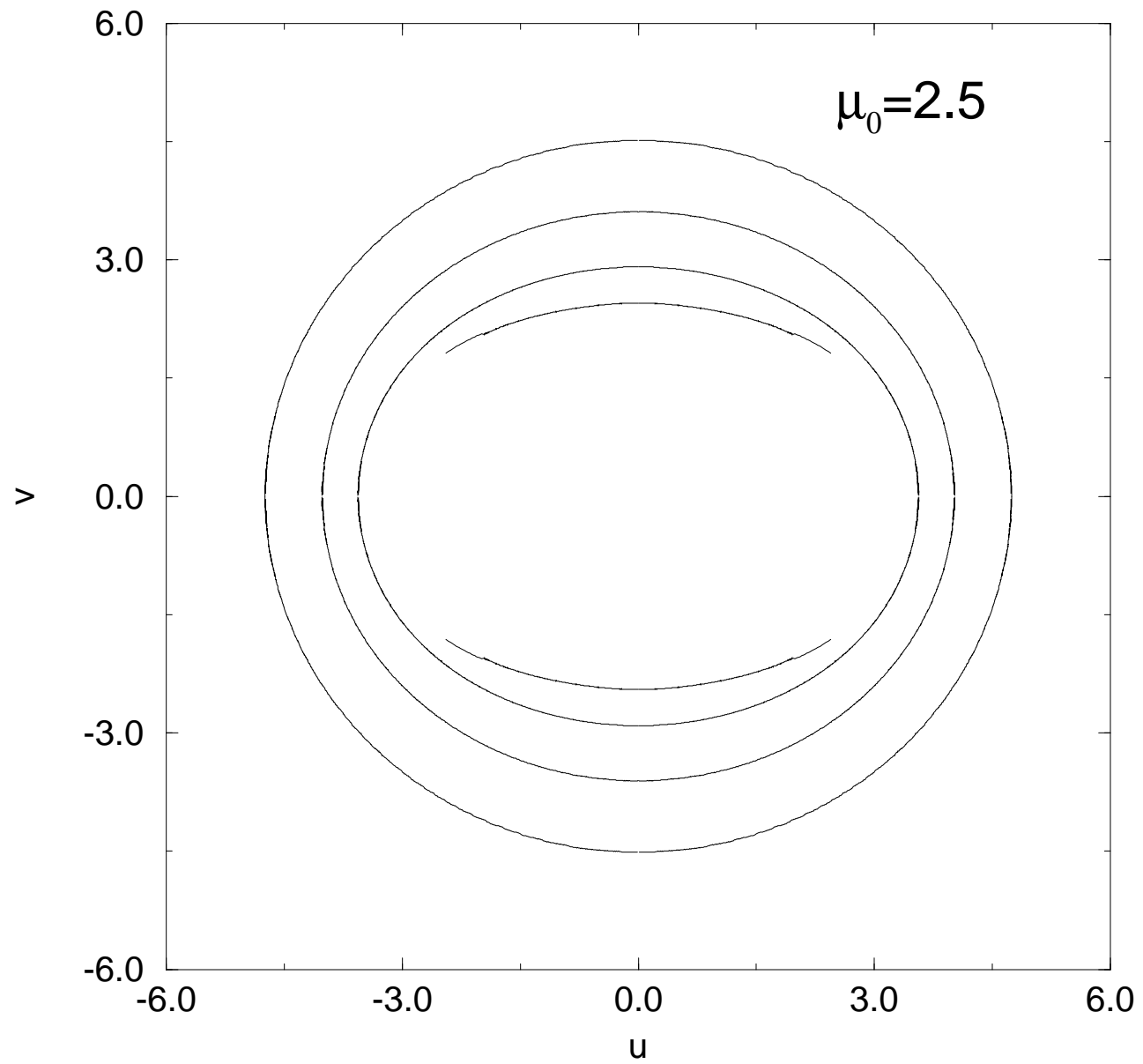


Figure 6c



This figure "fig1-7.png" is available in "png" format from:

<http://arxiv.org/ps/gr-qc/9409047v1>

This figure "fig1-8.png" is available in "png" format from:

<http://arxiv.org/ps/gr-qc/9409047v1>

This figure "fig1-9.png" is available in "png" format from:

<http://arxiv.org/ps/gr-qc/9409047v1>

This figure "fig1-10.png" is available in "png" format from:

<http://arxiv.org/ps/gr-qc/9409047v1>



This figure "fig1-11.png" is available in "png" format from:

<http://arxiv.org/ps/gr-qc/9409047v1>